On the Origin of Tropospheric Ozone and NO_x over the Tropical South Pacific

Martin G. Schultz[1], Daniel J. Jacob[1], Yuhang Wang[1,2], Jennifer A. Logan[1], Elliot Atlas[3], Donald R. Blake[4], Nicola J. Blake[4], John D. Bradshaw[5], Edward V. Browell[6], Marta A. Fenn[6], Frank Flocke[3], Gerald L. Gregory[6], Brian G. Heikes[7], Glen W. Sachse[7], Scott T. Sandholm[8], Richard E. Shetter[3], Hanwant B. Singh[9], and Robert W. Talbot[10]

submitted to JGR: 10/07/1997

for PEM-Tropics special section

revised: 06/08/1998

1. Dept. of Earth & Planetary Sciences, Harvard University, 29 Oxford St., Cambridge, MA02138, USA
2. now at Georgia Institute for Technology, Atlanta, GA
3. National Center for Atmospheric Research, Boulder, CO
4. University of California, Irvine, CA
5. deceased
6. NASA Langley reasearch Center, Hampton, VA
7. University of Rhode Island, Narragansett, RI
8. Georgia Institute for Technology, Atlanta, GA
9. NASA Ames Research Center, Wallops,
10. University of New Hampshire, Durham, NH

Abstract

The budgets of ozone and nitrogen oxides (NO_x = NO + NO_2) in the tropical South Pacific troposphere are analyzed by photochemical point modeling of aircraft observations at 0-12 km altitude from the PEM-Tropics A campaign flown in September-October 1996. The photochemical point model reproduces the observed NO_2/NO concentration ratio to within 30%, and has similar success in simulating observed concentrations of peroxides (H_2O_2, CH_3OOH), lending confidence in its use to investigate ozone chemistry. It is found that chemical production of ozone balances only half of chemical loss in the tropospheric column over the tropical South Pacific. The net loss is $1.8 \cdot 10^{11}$ molec./cm^2/s. The missing source of ozone is matched by westerly transport of continental pollution into the region. Independent analysis of the regional ozone budget with a global 3-dimensional model corroborates the results from the point model and reveales the importance of biomass burning emissions in South America and Africa for the ozone budget over the tropical South Pacific. In this model, biomass burning increases average ozone concentrations by 7-8 ppbv throughout the troposphere. The NO_x responsible for ozone production within the South Pacific troposphere below 4 km can be largely explained by decomposition of peroxyacetylnitrate (PAN) transported into the region with biomass burning pollution at higher altitudes.

1. Introduction

Ozone in the tropical troposphere is a major global source of OH radicals and hence plays an important role in maintaining the oxidizing power of the atmosphere [*Thompson*, 1992]. Ozone is produced in the troposphere by photochemical oxidation of CO and hydrocarbons in the presence of nitrogen oxide radicals (NO_x = NO + NO_2). NO_x is in general a limiting precursor for ozone production [*Chameides et al.*, 1992]. Loss of ozone is principally by photolysis and by chemical reactions with OH and HO_2. Several aircraft campaigns of the NASA Global Tropospheric Experiment (GTE) program have focused on improving our understanding of ozone chemistry and the resulting ozone budget in different regions of the tropical troposphere [*Harriss et al.*, 1988, 1990; *Hoell et al.*, 1996, 1997; *Fishman et al.*, 1996]. The latest of these campaigns, the Pacific Exploratory Mission - Tropics A (PEM-Tropics A), surveyed the distributions of ozone, NO_x, CO, hydrocarbons, and related species over the tropical South Pacific in September-October 1996 [*Hoell et al.*, this issue]. We present here a photochemical model analysis of the PEM-Tropics data aimed at constructing a budget of ozone and NO_x for the South Pacific troposphere and understanding the links to other regions of the tropical troposphere.

The South Pacific is the region of the tropical troposphere most remote from human activity. Tropospheric ozone columns are the lowest in the world, with values as low as one third those found in polluted regions of the tropics [*Fishman et al.*, 1990; *Kirchhoff et al.*, 1991; *Fishman and Brackett, 1997*]. The timing of PEM-Tropics corresponded to the end of the dry season in the southern tropics, when considerable biomass burning takes place in South America, Africa, and Oceania. The GTE/TRACE-A campaign conducted in September 1992 [*Fishman et al.*, 1996] demonstrated that biomass burning in southern Africa and Brazil causes seasonal enhancements in tropospheric ozone by a factor of 2 over the tropical South Atlantic [*Olson et al.*, 1996; *Thompson et al.*, 1996]. The TRACE A observations confirmed previous evidence of large-scale biomass burning pollution over the tropical South Atlantic from satellite observations of ozone and CO [*Fishman et*

al., 1990; *Watson et al.*, 1990]. *Fishman et al.* [1991] proposed that long-range transport of biomass burning pollution would affect ozone on a hemispheric scale. A major objective of PEM-Tropics A was to determine the extent of seasonal biomass burning influence over the South Pacific.

In addition to biomass burning, natural sources of NO_x from soils and lightning contribute to ozone formation in the tropical troposphere. Using the first aircraft observations of NO_x over the South Pacific, *Liu et al.* [1980] proposed a self-sustaining model for ozone in the tropical troposphere where net production of ozone in the upper troposphere balances net loss in the lower troposphere. Ozone production in their model was sustained by transport of NO_x from the stratosphere, which is now known to be negligibly small [*Kasibhatla et al.*, 1991; *Penner et al.*, 1991; *Lamarque et al.*, 1996]. More recent aircraft observations of NO_x in the tropical troposphere have demonstrated major primary sources from lightning [*Drummond et al.*, 1988; *Smyth et al.*, 1996; *Crawford et al.*, 1997], soils [*Jacob and Wofsy*, 1988, 1990], and biomass burning [*Andreae et al.*, 1988; *Singh et al.*, 1996b; *Smyth et al.*, 1996]. A notable feature of these three NO_x sources is that they are all continental (lightning over the oceans is extremely infrequent).

A photochemical model analysis of the TRACE-A observations [*Jacob et al.*, 1996] indicated a chemical balance for ozone on the scale of the tropospheric column. On the basis of this analysis, *Jacob et al.* [1996] proposed a schematic for the ozone budget in the tropical troposphere where NO_x pumped convectively over the tropical continents (upwelling branches of the Walker circulation) promotes ozone production in the upper troposphere, to be balanced by ozone depletion in the lower troposphere after the air subsides over the subtropical anticyclones (downwelling branches of the Walker circulation). A global 3-dimensional model analysis by *Wang et al.* [1998c] finds a close balance between zonal mean production and loss of ozone in the tropical troposphere, suggesting that the tropical troposphere is self-sustaining with respect to ozone, at least on a zonal scale.

The budget of ozone in the troposphere is strongly linked to that of NO_x. Considering that the lifetime of NO_x with respect to oxidation to HNO_3 is only of the order of 1 day, one would expect NO_x concentrations to decay rapidly downwind of the continents. However, observations over the tropical oceans indicate free tropospheric NO_x concentrations of typically 10-50 pptv [*Carroll and Thompson*, 1995; *Emmons et al.*, 1997], which play a major role in ozone production and are much higher than would be expected from direct transport of primary NO_x from the continents. It has been proposed that chemical recycling of NO_x from HNO_3 and other non-radical reservoirs, including in particular peroxyacetylnitrate (PAN), could play a major role in maintaining NO_x concentrations over the oceans [*Singh*, 1987]. However, previous photochemical model analyses of observations in the tropical marine troposphere concluded that chemical recycling based on known reactions was insufficient to maintain NO_x concentrations at their observed levels, and speculated on the possibility of fast conversion of HNO_3 to NO_x in aerosols [*Chatfield*, 1994; *Hauglustaine et al.*, 1996; *Jacob et al.*, 1996; *Lary et al.*, 1997].

2. Data summary

Two aircraft participated in the PEM-Tropics A campaign, a DC-8 and a P-3B. Both carried instrumentation for measurement of ozone, NO, CO, hydrocarbons, peroxides, and a number of other species. The DC-8 included measurements of PAN and HNO_3 and had a higher ceiling (12 km altitude, as compared to 7 km for the P-3B). The analysis here focuses on the DC-8 data.

The DC-8 operated from four bases: Tahiti, Easter Island, Christchurch (New Zealand), and Fiji. Sorties out of these bases examined the chemical composition of the South Pacific troposphere over a domain stretching from the warm pool of the equatorial Pacific to the subsiding region of the tropical eastern Pacific, and from the intertropical convergence zone (ITCZ) to high southern latitudes (Figure 1). The ITCZ was found in transit flights to be located at 7˚-9˚N.

Tables 1a,b list median concentrations of ozone, NO_x, PAN, HNO_3, peroxides, CO, and selected hydrocarbons observed at different altitudes in the equatorial and tropical South Pacific. We divide the data into two latitude bands, 0-10˚S and 10˚S-30˚S, because of the pronounced differences in ozone and CO concentrations (Figure 2) (see also [*Gregory et al.*, this issue]). Figure 3 compares the observations from PEM-Tropics A in the latitude band 0-30ºS to previous tropical data collected in the same season over the northwestern Pacific (PEM-West A) [*Hoell et al.*, 1996] and over the south Atlantic (TRACE A) [*Fishman et al.*, 1992]. While the vertical profiles of ozone and PAN (both photochemical products) from PEM-West A fall on the low end of the PEM-Tropics data, the profiles of CO and ethane (tracers for urban/industrial pollution or biomass burning) are shifted to somewhat higher concentrations. The data from TRACE A exhibit higher concentrations for several observed species. The largest differences are found for PAN: above 2 km, the TRACE A PAN concentration is at least a factor 4 higher than in the other two data sets.

The statistical distribution of ozone and CO at 4-8 km during PEM-Tropics A is displayed in Figure 2 for the 5 geographical regions defined in Figure 1. Both species follow similar patterns. The cleanest air was observed over the western equatorial Pacific and north of the subtropical convergence zone (SPCZ). Here, median mixing ratios were 27-32 ppbv for ozone and 56-58 ppbv for CO. The variability is also very small: the central 50% of the data span a range of less than 10 ppbv. The highest median values for both species were found over the western tropical Pacific (south of the SPCZ), with values of 61 ppbv for ozone and 78 ppbv for CO. These data also show a large variability, indicating the influence of episodic pollution events. During PEM-Tropics A, several layers with continental pollution were encountered in westerly air flow which originated from biomass burning in Africa or South America [*Blake et al.*, 1998; *Fuelberg et al.*, this issue]. Figure 2 shows occasional ozone and CO mixing ratios in excess of 100 ppbv for the tropical western Pacific south of the SPCZ. Almost 25% of the data from this region had ozone mixing ratios above 80 ppbv. This pollution influence decreased from west to east, reflecting dispersion and photochemical decay.

3. Model description

We use the Harvard photochemical point model to reconstruct the photochemical environment along the DC-8 flight tracks. The model calculates diurnal steady state concentrations of radicals and chemical intermediates using as constraints the ensemble of observations from the aircraft. Diurnal steady state is defined by repeatability of concentrations over a 24h cycle. The chemical mechanism is based on the compilations of *DeMore et al.* [1997] and *Atkinson et al.* [1997] with updates (e.g. pressure-dependent quantum yields for acetone photolysis [*McKeen et al.*, 1997]). All model results were submitted to the NASA Langley DAAC archive and are also available from the GTE web site http://www-gte.larc.nasa.gov.

Actinic fluxes are calculated with a 6 stream discrete ordinate radiative transfer model for the Rayleigh scattering atmosphere [*Logan et al.*, 1981]. The overhead ozone column for the radiative transfer calculation is specified from daily TOMS observations of total ozone columns, subtracting the ozone column below the aircraft as measured by the DIAL instrument [*Browell et al.*] and interpolating when necessary. In order to account for cloud scattering and absorption, we scaled the actinic flux for each individual data point with the ratio of observed to clear sky modeled photolysis frequencies in two wavelength regimes: for wavelengths up to 310 nm a correction factor for j_{O1D} was applied, above 310 nm we used a correction factor for j_{NO2}. Median correction factors were 1.21 for j_{NO2} and 1.03 for j_{O1D}.

For model input the observations were merged over 60 second time intervals. Measurements with a higher sampling frequency were averaged. An observation was considered valid only when all mandatory species (O_3, NO_x, H_2O, CO, HNO_3, PAN, peroxides) covered at least 25% of the interval. Observations of water vapor, CO, CH_4, HNO_3, PAN, peroxides, and non-methane

hydrocarbons were interpolated for a maximum of five minutes when necessary; remaining gaps in CH_4, HNO_3, PAN, and non-methane hydrocarbons were substituted by median values from table 1b. For the analysis of the NO_x budget (section 6) we used the time resolution of the HNO_3 measurements which had the longest integration times, and we only considered time intervals with observations of both PAN and HNO_3.

For water vapor we used measurements from the DACOM instrument [*G.Sachse, S. Vay*] (available in 70% of all cases) and from the cryogenically chilled mirror [*J. Barrick*]. Although both measurements agree on average within 20%, for mixing ratios below 100 ppmv the cryogenically chilled mirror tends to be lower by a factor of 2 to 5. This can be explained partly by the fact that the chilled mirror has a longer response time and seems to undershoot when the aircraft encounters dry air [*J. Barrick*, personal communication, 1997]. The DACOM data appear to be more reliable especially in the upper troposphere. However, the relative humidity derived from the DACOM data often exceeds 100% below 220 K, which would indicate a positive bias.

Acetone can act as the major primary source for hydrogen oxide radicals (HO_x = OH + peroxy species) in the upper troposphere [*Singh et al.*, 1995, *Jaeglé et al.*, 1997, *McKeen et al.*, 1997, *Arnold et al.*, 1997]. Since there were no measurements of acetone, we prescribed a constant acetone mixing ratio of 0.4 ppbv as a typical value for the southern tropics [*Wang et al.*, 1998b].

Except for NO, all input variables to the model calculation are assumed constant over the diurnal cycle. Because of the rapid cycling between NO and NO_2, we specify instead total NO_x^t (= NO + NO_2 + NO_3 + 2 N_2O_5 + HNO_4 + HONO) as constant and calculate the concentrations of the NO_x^t components as time-dependent variables over the diurnal cycle [*Jacob et al.*, 1996]. The concentration of NO_x^t is adjusted iteratively to match the observed NO concentration at the local time of the observation. Observations of NO_2 are not used to constrain the model and serve instead for model evaluation (section 4).

The chemical mechanism contains three heterogeneous reactions:

$$N_2O_5 + H_2O \rightarrow 2\ HNO_3, \quad \gamma = 0.1 \qquad \text{(R1)}$$

$$NO_3 + H_2O \rightarrow HNO_3, \quad \gamma = 0.01 \qquad \text{(R2)}$$

$$HO_2 + H_2O \rightarrow HO_2 \bullet H_2O$$
$$HO_2 \rightarrow H_2O_2 + O_2 + H_2O, \quad \gamma = 0.1 \qquad \text{(R3)}$$

The reaction probabilities γ follow the recommendations of *Jacob* [1998] with the upper limit for *(R2)*. The aerosol surface area was estimated from the condensation nuclei (0.004-1 μm) measurements [*Anderson*] using mean correlations between surface area and number density of aerosols (0.007-6 μm) measured aboard the P-3 aircraft [*Clarke*] in two altitude regimes.

Due to the requirement of concurrent measurements of NO, peroxides, and CO, model results are available only for about 40% of the PEM-Tropics A flight period. We checked the representativeness of the model data set in various regions of the South Pacific by comparing plots of the frequency distribution of the key species NO, O_3, H_2O, H_2O_2, CH_3OOH from both the complete observational and the model data set in altitude bands of 2 km. Most species compare well in all regions except above 10 km where sampling of some species is relatively sparse: in that altitude range the model data have significant low biases for NO (factor 0.48) over the central tropical Pacific, and for ozone (factor 0.55) over the western tropical Pacific south of the SPCZ. There are no model data above 10 km in the eastern tropical Pacific.

A different aspect of representativeness is the question of whether the PEM-Tropics observations represent average conditions for the southern Pacific troposphere in September. While the meteorological data indicate that temperatures and flow patterns in 1996 were close to the climatological mean [*Fuelberg et al.*, this issue], the ozonesonde data from Christchurch and Tahiti exhibit

some record high values during the time of the expedition [*J. Logan*, personal communication, 1997].

4. Cycling of NO and NO_2

Comparisons between modeled and observed NO_2/NO concentration ratios have been used previously to evaluate NO_x photochemistry in models and to assess the quality of the NO_2 measurements [e.g. *Chameides et al.*, 1990; *Davis et al.*, 1993; *Schultz*, 1995; *Crawford et al.*, 1996]. Many previous studies found that model calculated NO_2/NO ratios are systematically lower than observed ratios by a factor of about 1.5. This discrepancy showed a tendency to increase for cleaner air, i.e. closer to the limit of detection (LOD) for the NO_x measurements [*Schultz*, 1995; *Crawford et al.*, 1996]. In PEM-West A, *Crawford et al.* [1996] found a median ratio of experiment to theory of 3.3. Their analysis led to the conclusion that the measurement of NO_2 which was made with an older version of the two photon laser induced fluorescence (TP-LIF) instrument [*Bradshaw et al.*, 1985, *Sandholm et al.*, 1990] was prone to interferences with other photolabile NO_y compounds. For PEM-Tropics, the TP-LIF technique was improved by installing two new lasers with enhanced power, and by increasing the air flow. For the photodissociation of NO_2, the previously used Xenon lamp was replaced by a pulsed laser. All three improvements were expected to reduce wall losses and interference effects on the NO_2 measurement [*S. Sandholm*, personal communication, 1997].

Figure 4 displays the ratio of the modeled vs. observed NO_2/NO ratio in PEM-Tropics A as a function of altitude. Only data with NO_2 photolysis frequencies (j_{NO2}) greater than $7 \cdot 10^{-3}$ s^{-1} were used in order to prevent a possible bias from incorrect NO_x estimates in the point model. The model calculated NO_2/NO ratios are generally too high by about 10%. This is well within the stated uncertainties of the measurements of NO_2 and j_{NO2} (20-30% and 10%, respectively).

Below 2 km, a systematic negative bias of about 20% is observed which is still within the stated uncertainties, especially since NO_x concentrations were very low. However, halogen chemistry in the marine boundary layer could also cause this bias. We were able to reconcile the modeled NO_2/NO ratio with the observations below 2 km by introducing a chlorine atom concentration of 10^5 molec./cm^3 as suggested from observations of hydrocarbon ratios over the tropical western Pacific [*Singh et al.*, 1996a]. Under these conditions, the ClO + NO reaction is a significant pathway converting NO to NO_2. Sensitivity calculations with BrO levels of 10^7 molec./cm^3 [*Vogt et al.*, 1996] or I_x (= HOI + HI + IO + I + minor components) concentrations of $3.8 \cdot 10^7$ molec./cm^3 [*Davis et al.*, 1996b] showed no significant effect on the NO_2/NO ratio.

5. Peroxides

The peroxides H_2O_2 and CH_3OOH are produced by recombination of peroxy radicals and have lifetimes of 1-2 days with respect to photolysis and reaction with OH for the PEM-Tropics A conditions. One would therefore expect H_2O_2 and CH_3OOH to be in general near chemical steady state, and the ability of the model to reproduce this steady state provides a test for the peroxy radical concentrations and hence the ozone production rates calculated by the model. In our calculations, we use the observed peroxide concentrations as model constraints and examine the resulting imbalance between photochemical loss and photochemical production as diagnostic of departure from steady state. This approach has the advantage of not imposing the assumption of steady state for peroxides on the calculation of HO_x concentrations.

Figure 5 shows the balance of simulated 24h averaged chemical loss and production rates for H_2O_2 and CH_3OOH as a function of altitude. Between 2 and 8 km the balance is generally within 10% for H_2O_2 and 15% for CH_3OOH. Below 2 km, the agreement is still within 10% for CH_3OOH, but results for H_2O_2 indicate a missing

sink of magnitude comparable to chemical loss. This missing sink can be attributed to wet and dry deposition, which is not included in the point model. Above 8 km, the scatter increases substantially, and the model underestimates the source of CH_3OOH by 40-130% while the H_2O_2 budget remains balanced within 10-40% on average. Deep convection elevates CH_3OOH in the upper troposphere above chemical steady state, while having little impact on H_2O_2 due to scavenging by the convective precipitation [*Prather and Jacob*, 1997; *Jaeglé et al.*, 1997]. During PEM-Tropics A, *Cohan et al.* [this issue] found that CH_3OOH concentrations in deep convective outflow at 8-12 km altitude were elevated by a factor of 6 relative to background, while H_2O_2 concentrations were elevated only by 50%. Using CH_3I as a chemical clock, they estimated a timescale of 2-3 days for the decay of the convective enhancement of peroxides in the upper troposphere; this timescale is still relatively short compared to the 10 day turnovertime for the upper troposphere [*Prather and Jacob*, 1997].

Therefore, it does not appear that convective transport alone can explain the imbalance in the CH_3OOH budget in Figure 5. Another contributing factor could be an underestimate of the rate constant for the CH_3O_2+HO_2 reaction which is uncertain by about a factor of 3 at temperatures around 220 K [*DeMore et al.*, 1997].

Previous studies of the PEM-West and TRACE-A data [*Davis et al.*, 1996a; *Jacob et al.*, 1996; *Crawford*, 1997] calculated peroxide concentrations from chemical steady state and compared these to the observations. *Jacob et al.* [1996] report a significant underestimate of H_2O_2 model concentrations (median ratios of model/observed of 0.99, 0.87, and 0.57 in the altitude bins 0-4, 4-8, and 8-12 km), and an even worse imbalance for CH_3OOH (ratios are 0.59, 0.79, and 0.28). For PEM-West B, the model of *Crawford* [1997] typically overestimates H_2O_2 by about 30% in the equatorial region below 10 km, except for the surface layer where deposition plays a role. On the other hand, CH_3OOH is generally predicted within about 20% up to 8 km, and it is underpredicted by a factor of 2.4 and 5 in the altitude bins of 8-10 km and 10-12 km, respectively. For PEM-West A, *Davis et al.* [1996a] give only one median value for the ratio of observed to modeled peroxide concentrations above 1 km (0.92 for H_2O_2 and 0.62 for CH_3OOH). With the exception of *Jacob et al.* [1996] all these studies indicate that a photochemical steady state model can successfully simulate H_2O_2 in the free troposphere, whereas CH_3OOH is systematically underestimated by the models above 8 km.

6. Sources and sinks of NO_x

The lifetime of NO_x with respect to photochemical loss, as calculated by our photochemical model for PEM-Tropics A conditions, is 1-5 days for most of the tropical South Pacific troposphere (Table 2). The PEM-Tropics study region is sufficiently far from most known primary sources of NOx (fossil fuel combustion, biomass burning, soil emissions, lightning), that we would expect NO_x to be generally near chemical steady state, maintained by recycling of HNO_3 and PAN.

Figure 6 displays mean modeled NO_x budgets for the equatorial and tropical region, constrained with observations of NO, PAN, and HNO_3. The chemical mechanism of the model takes into account the cycling between NO, NO_2, HNO_3, PAN, and HO_2NO_2. Methyl nitrate is also included as NO_x source, because observations of several pptv even above 6 km suggested it might be important under conditions of very low HNO_3 and PAN [*F. Flocke*, personal communication, 1997]. We corrected the rates for production and loss of PAN at every time step as described in [*Jacob et al.*, 1996].

Thermal decomposition of PAN is the dominant production term for NO_x below 4 km, closely balancing the loss of NO_x (Figure 6). We conclude that PAN provides the main source of NO_x at these altitudes. Long-range transport of biomass burning pollution was a major source of PAN over the tropical South Pacific during PEM-Tropics A, as shown in Figure 7 by the correlation between PAN and C_2H_2 at 4-8 km.

Above 4 km, we find that the chemical source of NO_x is insufficient to balance the loss of NO_x from oxidation, implying a large missing source for NO_x. Such a chemical imbalance in the upper troposphere has been found in previous missions [e.g. *Davis et al.*, 1996a*; Jacob et al.*, 1996]. Recent studies by *Jaeglé et al.* [1998], *Prather and Jacob* [1997], and *Wang et al.* [1998b] suggest that this imbalance is mostly caused by convective injection and primary production of NO_x from lightning. However, *Wang et al.* [1998b] find evidence of a missing chemical source of NO_x in tropical regions where biomass burning is of importance. Further analysis of the PEM-Tropics A data [*Schultz et al.*, manuscript in preparation 1998] suggests that large amounts of ammonia emitted by biomass burning may slow down the loss of NO_x by dehydrating the aerosol, while also providing an additional chemical source of NO_x, thus correcting most of the NO_x budget imbalance apparent from Figure 6.

7. Ozone formation and loss rates

Figure 8 displays median production and loss rates of odd-oxygen ($O_x = O_3 + O + NO_2 + HNO_4 + 2{\cdot}NO_3 + 3{\cdot}N_2O_5 + HNO_3 + PAN + PPN$) as a function of altitude for the equatorial and tropical South Pacific. The chemical budget analysis must be applied to O_x, rather than to O_3, because of the fast chemical cycling within the O_x family. Considering that ozone makes up more than 90% of O_x for the PEM-Tropics A conditions, we will use both terms interchangeably. During PEM-Tropics A, the lower 4 km of the troposphere over the tropical South Pacific exhibit net destruction rates of about 2 ppbv/day for ozone while there is about 1 ppbv/day net production above 8 km. The crossover at 6 km is similar to results from PEM-West A and B [*Davis et al.*, 1996a; *Crawford*, 1997].

The geographical distribution of ozone production (Plate 1) shows highest values over the western tropical Pacific where biomass burning influence is strongest (Figure 2). As shown in Table 3, chemical production of ozone balances only about half of the chemical loss for the 0-12 km column over the South Pacific; the column integrated net loss amounts to about $1\text{-}2{\cdot}10^{11}$ molec./cm^2/s which is equivalent to 0.35-0.7 Dobson units (DU) per day. This result does not change significantly when we extrapolate the data to the tropopause height of about 16 km (Table 3).

Above 4 km the rates of ozone production and loss over the South Pacific are similar to those computed for the northern tropical Pacific during PEM-West A (Figure 10). Compared to the troposphere over the tropical South Atlantic during TRACE A, production and loss rates over the tropical Pacific are a factor of 2-5 lower.

Our analysis of the photochemical budget for hydrogen peroxides (section 5) revealed some uncertainty regarding the HO_x budget in the upper troposphere. In order to investigate the implications on the calculated budget of ozone, we performed a series of sensitivity simulations, using as reference a simulation constrained by median observed values in the tropical latitude band for the altitude bins of 8-10 km and 10-12 km (Table 1b). In these calculations water vapor was varied by a factor of 2, the rate coefficient for the HO_2+CH_3O_2 reaction was varied by a factor of 3, and the acetone concentration was varied from 400 pptv to 50 pptv. From the combination of effects the maximum deviations for P_{O3} and L_{O3} were 35%. The deviation of $(P\text{-}L)_{O3}$ was smaller (-22% to +9%).

Let us now investigate whether the advection of continental air can balance the large observed ozone loss in the South Pacific troposphere. Layers of continental air sampled during PEM-Tropics A contained elevated CO due to pervasive biomass burning on the south tropical continents [*Blake et al.*, 1998]. The mean enhancement ratio $\Delta O_3/\Delta CO$ in these layers was 1.8 mol/mol [*Logan*, personal communication 1997], reflecting the fact that NO_x from continental sources (including biomass burning, lightning, and soil emissions) allowed considerable ozone production. Let us take $\Delta O_3/\Delta CO = 1.8$ mol/mol as a general characteristic of continental air advected over the South Pacific; then

$$\nabla F_{O3} = \nabla F_{CO}(\Delta O_3/\Delta CO) \qquad (1)$$

where ∇F_{O3} and ∇F_{CO} are the flux divergences of O_3 and CO over the South Pacific, i.e. the net influx into the region. The net influx of CO is exclusively from continental pollution. We write a mass balance equation for CO in the tropospheric column over the South Pacific,

$$\nabla F_{CO} + (P\text{-}L)_{CO} = 0 \qquad (2)$$

where $(P\text{-}L)_{CO}$ is the net production of CO over the South Pacific as determined from our photochemical model analysis (Table 6). In equation (2) we have ignored the CO tendency term, which is negligibly small. Equation (2) yields $\nabla F_{CO} = 1.6 \cdot 10^{11}$ molec./cm^{2}s (Table 3, results for 0-16 km); replacing into equation (1) we obtain $\nabla F_{O3} = 2.9 \cdot 10^{11}$ molec./cm^{2}s. Comparing to the net column loss of ozone over the South Pacific computed from our photochemical model analysis, $(L\text{-}P)_{O3} = 0.9 \cdot 10^{11}$ molec./cm^{2}s, we conclude that advection of continental air can readily account for the net influx of tropospheric ozone over the tropical South Pacific. The $\Delta O_3/\Delta CO$ ratio used in our calculation is certainly too high because the aircraft undersampled continental air advected in the lower troposphere from South America, which had a low $\Delta O_3/\Delta CO$ ratio due to fast chemical loss of ozone. A mean $\Delta O_3/\Delta CO$ ratio of 0.6 mol/mol for continental air advected over the South Pacific would close the ozone budget and is in the range of expected values.

Our analysis above indicates that ozone production over the South Pacific driven by influx of PAN and direct influx of ozone from tropical continental regions both provided major sources for ozone in the South Pacific troposphere during PEM-Tropics A. It appears likely that biomass burning made a dominant contribution to both of these sources. Ozone and PAN concentrations measured in the free troposphere over Brazil and Africa during TRACE-A were considerably higher than in PEM-Tropics A (Figure 3) and were due unambiguously to biomass burning [*Singh et al.*, 1996b; *Thompson et al.*, 1996]. Zonal transport at both tropical and subtropical latitudes [*Fuelberg et al.*, 1998] would supply this biomass burning ozone and PAN to the South Pacific troposphere. As mentioned previously, PAN in PEM-Tropics A was correlated positively with tracers of biomass burning (Figure 7). Although lightning could also have contributed to long-range transport of NO_x over the Pacific, year-round ozonesonde measurements at South Pacific sites [*Oltmans et al.*, personal communication, 1997] argue against a major contribution of lightning to ozone in PEM-Tropics A. The ozonesonde data show a pronounced seasonal maximum of ozone in austral spring, during the biomass burning season, consistent with ozonesonde data in the TRACE-A region [*Olson et al.*, 1996]. In contrast, lightning peaks in austral summer [*Turman and Edgar*, 1982].

8. Global 3D model simulation

In order to provide an additional perspective on the large-scale regional budget of ozone over the tropical South Pacific, we analyzed results from the Harvard/GISS global 3D model [*Wang et al.*, 1998a]. The model uses meteorological fields from the Goddard Institute for Space Sciences (GISS) Global Climate Model (GCM) and has 4°x5° horizontal resolution with 9 vertical layers, 7 of which are in the troposphere. A suite of 15 chemical tracers including O_3, NO_x, PAN, HNO_3, CO, H_2O_2, and five primary hydrocarbons is simulated, with parametrizations for tracer production and loss derived from point model simulations with a detailed mechanism over a wide range of conditions. Fossil fuel combustion, woodburning, and biomass burning emissions are from *J. Logan* [manuscript in preparation, 1998]. Biogenic emissions are parametrized similar to *Guenther et al.* [1995], and soil emissions are formulated according to *Yienger and Levy* [1995] and *Jacob and Bakwin* [1991]. The model has been extensively evaluated with observations [*Wang et al.*, 1998b].

Figure 3 compares model results (dashed lines) with the PEM-Tropics A observations (solid circles) for median concentrations of ozone, CO, and PAN. Ozone concentrations in the 3D model are lower than the observations below 3 km by 7 ppbv (30%), and they show a smaller enhancement near 6 km (the 25 percentile of the observations is close to the 95 percentile of the model). However, the general tendency is reproduced: median con-

centrations of ozone are largest around 6 km. The simulated vertical profile of CO agrees with the observations within 5 ppbv. As in the case of ozone, the variability of the observations is significantly larger than the variability in the 3D simulation below 4 km. The vertical profile of PAN is also predicted within one standard deviation of the observations; the model concentrations are about 20% higher.

The rates of photochemical ozone formation and loss calculated with the global model agree with those from the point model within 20% (Figure 8). Ozone loss below 2 km and production above 6 km are somewhat higher in the point model. The geographical distribution of ozone production rates (Plate 2) is similar in both models. Both show enhanced ozone production above 4 km in the western Pacific around 15˚ S due to advection of continental air. The global model also predicts enhanced ozone production over the eastern equatorial Pacific (Plate 2), indicating outflow of pollution from South America. Data from the P-3B aircraft flights along the western coast of South America indicate that easterly continental outflow can have biomass burning as a major component [*N. Blake*, personal communication, 1997].

Table 4 lists the individual terms that contribute to the 3D model budget for ozone over the tropical South Pacific in September. The two altitude regimes (0-4.5 km and 4.5-13 km) reflect the transition from southeasterly trade winds to predominant westerly flow [e.g. *Fuelberg et al.*, this issue]. In the lower part of the troposphere, the ozone budget is dominated by advection from the east together with vertical downward transport, and by photochemical loss inside the region. In-situ formation of ozone balances only one third of the photochemical loss. Above 4.5 km, ozone is advected predominantly from the west; this term is about twice as large as the advection from the east in the lower part. The net downward vertical flux of $0.53 \cdot 10^{11}$ molec./cm^{2}s amounts to about 17% of the lateral outflux above 4.5 km to the east and south. For the entire 0-13 km column over the South Pacific, we find in the 3D model that 55% of the ozone originates from within the region and 45% is transported in the flux divergence term. This result is consistent with our point model analysis, where column integrated chemical production balanced 50% of the chemical loss (Table 3). Although not apparent from Table 4, a tracer analysis in the 3D model indicates that 20% of tropospheric ozone over the tropical South Pacific (0-30ºS) originates from cross-tropopause transport in the extratropical southern hemisphere [*Wang et al.*, 1998c].

In order to assess the impact of biomass burning on the ozone budget over the tropical South Pacific, we conducted a 3D model simulation without biomass burning emissions. Ozone mixing ratios from both simulations are compared in Figure 9. September mean ozone mixing ratios over the tropical South Pacific (0º-28ºS; 165ºE-100ºW) are on average higher by 7 and 8 ppbv (~20%) respectively for altitudes below and above 4.5 km. Without biomass burning, influx from the east at lower altitudes decreases by almost a factor of two, while the advection from the west above 4.5 km decreases by 30% (Table 4). Photochemical production above 4.5 km now exceeds loss by almost a factor of 2, but the absolute difference between these two terms remains about the same. In general, the chemical terms decrease proportionally to the advection terms, supporting our finding that biomass burning pollution affects advection of ozone as well as in situ production over the South Pacific.

At first sight, these simulations suggest that biomass burning in South America impacts ozone below 4.5 km, whereas source regions to the west (Africa and South America) contribute to ozone advection and formation above. However, as discussed in section 6, the abundance of NO_x in the lower troposphere is controlled by thermal decomposition of PAN which is advected above 4 km as part of the biomass burning pollution. Because of the warm temperatures and the availability of UV radiation, the lifetimes of NO_x and PAN are too short to allow significant transport of these species in the trade winds at lower altitudes. This implies that the chemical ozone formation in the lower troposphere is controlled by downward transport of precursors that have been advected from the west. This is supported by the difference in subsidence fluxes of PAN between the two simulations: without biomass burning emissions, this flux is a factor

of three lower. Adding the vertical transport of ozone to the chemical formation of ozone in the lower troposphere, we find that the sum is comparable in magnitude with the horizontal advection of ozone from the east (Table 4). Hence, biomass burning pollution advected from the west can account for all the biomass burning ozone enhancement above 4.5 km and for half of the increase at lower levels. Biomass burning pollution advected from the east affects ozone only in the lower troposphere over eastern South Pacific.

9. Summary

The model analysis of the PEM-Tropics A data from the DC-8 revealed the important contribution of biomass burning to the ozone budget over the tropical South Pacific. PEM-Tropics A took place during the burning season, and it will be interesting to compare these results to the data of PEM-Tropics B which is scheduled for the rain season in February-March 1999. Both, the point model and the Harvard/GISS global 3D model, calculate a photochemical column net loss for ozone of about $1.5 \cdot 10^{11}$ molec.cm^{-2}s^{-1} during PEM-Tropics A. Photochemical production of ozone balances about half of the chemical loss; the ozone budget can be closed with advection of continental air. The turnover from net photochemical loss to net photochemical production takes place around 6 km, as was previously found for the tropical South Atlantic in TRACE A and for the tropical North Pacific in PEM-West A and B.

The ozone budget in the lower 4 km of the South Pacific troposphere is largely affected by PAN that is advected in biomass burning pollution layers at higher altitudes. Below 4 km, the thermal decomposition of PAN can account for most of the NO_x production, and it therefore controls chemical ozone formation. Subsidence of ozone from above and photochemical production contribute as much to the ozone budget in the lower troposphere as advection of biomass burning pollution from South America in easterly trade winds. The comparison of a global 3D simulation with and without biomass burning emissions showed that biomass burning caused an increase in ozone concentrations over the tropical South Pacific of 7-8 ppbv at all altitudes.

Acknowledgments. We would like to thank C. Spivakovsky for her continous effort to develop and maintain the point model, L. Jaeglé for helpful discussions and the update of the chemical mechanism of the point model, and G. Gardner for help in preparing the merged data sets. We also thank J. Crawford for providing data for PEM-West A, and J. Barrick for helpful discussions on the measurements of water vapor. The work of M. Schultz was funded by the Deutsche Forschungsgemeinschaft (DFG), PEM-Tropics was funded as part of the NASA GTE program.

References

Andreae, M.O., et al., Biomass-burning emissions and associated haze layers over Amazonia, *J. Geophys. Res., 93*, 1509-1527, 1988.

Arnold, F., V. Brüger, B. Droste-Fanke, F. Grimm, A. Krieger, J. Schneider, and T. Stilp, Acetone in the upper troposphere and lower stratosphere: Impact on trace gases and aerosols, *Geophys. Res. Lett., 24*, 3017-3020, 1996.

Atkinson R., D.L. Baulch DL., R.A. Cox, R.F. Hampson, J.A. Kerr, M.J. Rossi, J. Troe, Evaluated kinetic and photochemical data for atmospheric chemistry - Supplement VI, *J. Phys. Chem. Ref. Data, 26(6)*, 1329-1499, 1997.

Blake, D.R., *** ET AL. ***, The impact of biomass burning on the remote south Pacific troposphere, submitted to *Science*, 1998.

Bradshaw, J.D., M.O. Rodgers, S.T. Sandholm, S. KeSheng, and D.D. Davis, A two-photon laser-induced fluorescence field instrument for ground-based and airborne measurements of atmospheric NO, *J. Geophys. Res., 90/D7*, 12,861-12,873, 1985.

Carroll, M.A., and A.M. Thompson, NOx in the non-urban troposphere, in *Progress and Problems in Atmospheric Chemistry*, ed. J. Barker, World Sci. Pub. Co., Singapore, 1995.

Chameides, W.L., et al., Observed and model calculated NO_2/NO ratios in tropospheric air sampled during the NASA GTE/CITE 2 field

study, *J. Geophys. Res., 95/D7*, 10,235-10,247, 1990.

Chameides, W.L., et al., Ozone precursor relationships in the ambient atmosphere, *J. Geophys. Res., 97*, 6037-6055, 1992.

Chatfield, R.B., Anomalous HNO_3/NO_x ratio of remote tropospheric air: conversion of nitric acid to formic acid and NO_x?, *Geophys. Res. Lett., 21*, 1994.

Cohan, D.S., M.G. Schultz, D.J. Jacob, B.G. Heikes, D.R. Blake, Convective injection and photochemical decay of peroxides in th etropical upper troposphere: Methyl iodide as a tracer of marine convection, *J. Geophys. Res.*, this issue.

Crawford, J., et al., Photostationary state analysis of the NO_2 -NO system based on airborne observations from the western and central north Pacific, *J. Geophys. Res., 101*, 2053-2072, 1996.

Crawford, J., An analysis of the photochemical environment over the western, north Pacific based on airborne field observations, PhD thesis, Georgia Insitute of Technology, 1997.

Crawford, J.H., et al., Implications of large scale shifts in tropospheric NO_x levels in the remote tropical Pacific, *J. Geophys. Res., 102/D23*, 28,477-28,468, 1997.

Davis, D.D., et al., A photostationary state analysis of the NO_2-NO system based on airborne observations from the subtropical/tropical North and South Atlantic, *J. Geophys. Res., 98*, 23,501-23,523, 1993.

Davis, D.D., et al., Assessment of ozone photochemistry in the western North Pacific as inferred from PEM-West A observations during the fall 1991, *J. Geophys. Res., 101/D1*, 2111-2134, 1996a.

Davis, D.D., J. Crawford, S. Liu, S. McKeen, A. Bandy, D. Thornton, F. Rowland, and D. Blake, Potential impact of iodine on tropospheric levels of ozone and other critical oxidants, *J. Geophys. Res., 101/D1*, 2135-2147, 1996b.

DeMore, W.B., S.P. Sander, D.M. Golden, R.F. Hampson, M.J. Kurylo, C.J. Howard, A.R. Ravishankara, C.E. Kolb, and M.J. Molina, Chemical kinetics and photochemical data for use in stratospheric modeling, *JPL publication 97-4*, NASA Jet Propulsion Laboratory, Pasadena, Calif., 1997.

Drummond, J.W., D.H. Ehhalt, and A. Volz, Measurements of nitric oxide between 0-12 km altitude and 67˚N to 60˚S latitude obtained during STRATOZ III, *J. Geophys. Res., 92*, 15,831-15,849, 1988.

Emmons, L.K., et al., Climatologies of NOx and NOy: A comparison of Data and Models, *Atmospheric Environment, 31*, 1851-1903, 1997.

Fan, S.-M., D.J. Jacob, D.L. Mauzerall, J.D. Bradshaw, S.T. Sandholm, D.R. Blake, H.B. Singh, R.W. Talbot, G.L. Gregory, and G.W. Sachse, Origin of tropospheric NO_x over subarctic eastern Canda in summer, *J. Geophys. Res., 99/D8*, 16,867-16,877, 1994.

Fishman, J., C.E. Watson, J.C. Larsen, and J.A. Logan, Distribution of tropospheric ozone determined from satellite data, *J. Geophys. Res., 95*, 3599-3617, 1990.

Fishman, J., K. Fakhruzzaman, B. Cros, and D. Nganga, Identification of widespread pollution in the southern hemisphere deduced from satellite analysis, *Science*, 252, 1693-1696, 1991.

Fishman, J., J.M. Hoell, R.D. Bendura, R.J. McNeal, and V.W.J.H. Kirchhoff, NASA GTE TRACE A Experiment (September-October 1992): Overview, *J. Geophys. Res., 101/D19*, 23,865-23,879, 1996.

Fishman, J., and V.G. Brackett, The climatological distribution of tropospheric ozone derived from satellite measurements using version 7 Total Ozone Mapping Spectrometer and Stratospheric Aerosol and Gas Experiment data sets, *J. Geophys. Res., 102/D15*, 19,275-19,278, 1997.

Fuelberg, H.E., R.E. Newell, S.P. Longmore, Y. Zhu, D.J. Westberg, E.V. Browell, D.R. Blake, G.R. Gregory, G.W. Sachse, A meteorological overview of the PEM-Tropics period, *J. Geophys. Res.*, this issue.

Gregory, G.L., D.J. Westberg, M.C. Shipham, D.R. Blake, R.E. Newell, R.W. Talbot, B.G. Heikes, G.W. Sachse, B.A. Anderson, and D.C. Thornton, Chemical characteristics of pacific tropospheric air in the region of the ITCZ and SPCZ, *J. Geophys. Res.*, this issue.

Guenther, A., et al., A global model of natural vol-

atile organic compound emissions, *J. Geophys. Res.*, *100*, 8873-8892, 1995.

Harriss, R. C. et al., The Amazon Boundary Layer Experiment (ABLE 2A): dry season 1985, *J. Geophys. Res.*, *93*, 1351-1360, 1988.

Harriss, R.C., et al., The Amazon Boundary Layer Experiment: wet season 1987, *J. Geophys. Res.*, *95*, 16,721-16,736, 1990.

Hauglustaine, D. A., B. A. Ridley, S. Solomon, P. G. Hess, and S. Madronich, HNO3/NOx ratio in the remote troposphere during MLOPEX 2: Evidence for nitric acid reduction on carbonaceous aerosols, *Geophys. Res. Lett.*, *23*, 2609-2612, 1996.

Hoell, J.M., D.D. Davis, S.C. Liu, R.E. Newell, M. Shipham, H. Akimoto, R.J. McNeal, R.J. Bendura, and J. W. Drewry, Pacific Exploratory Mission West-A(PEM West-A): September-October 1991. *J. Geophys. Res.*, *101/D2*, 1641-1653, 1996.

Hoell, J.M., D.D. Davis, S.C. Liu, R.E. Newell, H. Akimoto, R.J. McNeal, and R.J. Bendura, The Pacific Exploratory Mission-West Phase B: February-March, 1994, *J. Geophys. Res.*, *102/D23*, 28,223-28,240, 1997.

Hoell, J.M., *** ET AL. ***, The Pacific Exploratory Mission-Tropics Phase A: August-October 1996, *J. Geophys. Res.*, this issue.

Jacob, D.J., and P.S. Bakwin, Cycling of NO_x in tropical forest canopies and its implications for the global source of biogenic NO_x to the atmosphere, in *Microbiological Production and Consumption of Greenhouse Gases*, ed. W.B. Whitman, American Society of Microbiology, Washington, D.C., 1991.

Jacob, D.J., and S.C. Wofsy, Photochemistry of biogenic emissions over the Amazon forest, *J. Geophys. Res.*, *93*, 1477-1486, 1988.

Jacob, D.J., and S.C. Wofsy, Budgets of reactive nitrogen, hydrocarbons, and ozone over the Amazon forest during the wet season, *J. Geophys. Res.*, *95*, 16,737-16,744, 1990.

Jacob, D.J., B.G. Heikes, S.-M. Fan, J.A. Logan, D.L. Mauzerall, J.D. Bradshaw, H.B. Singh, G.L. Gregory, R.W. Talbot, D.R. Blake, and G.W. Sachse., Origin of ozone and NOx in the tropical troposphere: A photochemical analysis of aircraft observations over the South Atlantic basin, *J. Geophys. Res.*, *101*, 24,235-24,250, 1996.

Jacob, D.J., Heterogeneous chemistry and tropospheric ozone, submitted to *Atmospheric Environment*, March 1998.

Jaeglé, L., et al., Observed OH and HO_2 in the upper troposphere suggest a major source from convective injection of peroxides, *Geophys. Res. Lett.*, *24*, 3181-3184, 1997.

Jaeglé, L., D.J. Jacob, Y. Wang, A.J. Weinheimer, B.A. Ridley, T.L. Campos, G.W. Sachse, and D. Hagen, Origin of NOx in the upper troposphere over the central United States, *Geophys. Res. Lett.*, *25*, 1709-1712, 1998.

Kasibhatla, P.S., H. Levy, W.J. Moxim, and W.L. Chameides, The relative importance of stratospheric photochemical production on tropospheric NOy levels: a model study, *J. Geophys. Res.*, *96*, 18,631-18,646, 1991.

Kirchhoff, V.W.J.H., R.A. Barnes, and A.L. Torres, Ozone climatology at Natal Brazil, from in situ ozonesonde data, *J. Geophys. Res.*, *96*, 10,899-10,909, 1991.

Lamarque, J.-F., G.P. Brasseur, P.G. Hess, and J.-F. Muller, Three-dimensional study of the relative contributions of the different nitrogen sources in the troposphere, *J. Geophys. Res.*, *101*, 22,955-22,968, 1996.

Lary, D. J., A. M. Lee, R. Toumi, M. J. Newchurch, M. Pirre, and J. B. Renard, Carbon aerosols and atmospheric photochemistry. *J. Geophys. Res.*, *102*, 3671-3682, 1997.

Liu, S.C., D. Kley, M. McFarland, J.D. Mahlman, and H. Levy II, On the origin of tropospheric ozone, *J. Geophys. Res.*, *85*, 7546-7552, 1980.

Logan, J.A., M.J. Prather, S.C. Wofsy, and M.B. McElroy, Tropospheric chemistry: A global perspective, *J. Geophys. Res.*, *86/C8*, 7210-7254, 1981.

McKeen, S.A., T. Gierczak, J.B. Burkholder, P.O. Wennberg, T.F. Hanisco, E.R. Keim, R.-S. Gao, S.C. Liu, A.R. Ravishankara, and D.W Fahey, The photochemistry of acetone in the upper troposphere: A source of odd-hydrogen radicals, *Geophys. Res. Lett.*, *24*, 3177-3180, 1997.

Olson, J., J. Fishman, V.W.H.J. Kirchhoff, D. Nganga, and B. Cros, Analysis of the distribution of ozone over the southern Atlantic region, *J. Geophys. Res.*, *101*, 24,083-24,094, 1996.

Penner, J.E., C.S. Atherton, J. Dignon, S.J. Ghan, J.J. Walton, and S. Hameed, Tropospheric nitrogen: a three-dimensional study of sources, distributions, and deposition, *J. Geophys. Res., 96*, 959-990, 1991.

Prather, M.J., and D.J. Jacob, A persistent imbalance in HO_x and NO_x photochemistry of the upper troposphere driven by deep tropical convection, *Geophys. Res. Lett., 24(24)*, 3189-3192, 1997.

Sandholm, S.T., J.D. Bradshaw, K.S. Dorris, M.O. Rodgers, and D.D. Davis, An airborne compatible photofragmentation two-photon laser-induced fluorescence instrument for measuring background tropospheric levels of NO, NOx, and NO_2, *J. Geophys. Res., 95/D7*, 10,155-10,161, 1990.

Schultz, M., Die Bedeutung von Stickoxiden für die Ozonbilanz in Reinluftgebieten, PhD thesis, University of Wuppertal/Germany, 1995.

Singh, H.B., Reactive nitrogen in the troposphere, *Environ. Sci. Technol., 21*, 320-327, 1987.

Singh, H.B., M. Kanakidou, P.J. Crutzen, and D.J. Jacob, High concentrations and photochemical fate of oxygenated hydrocarbons in the global troposphere, *Nature*, 378, 50-54, 1995.

Singh, H.B., et al., Low ozone in the marine boundary layer of the tropical Pacific ocean: Photochemical loss, chlorine atoms, and entrainment, *J. Geophys. Res., 101/D1*, 1907-1917, 1996a.

Singh, H.B., et al., Impact of biomass burning emissions on the composition of the South Atlantic troposphere: Reactive nitrogen and ozone, *J. Geophys. Res., 101/D19*, 24,203-24,220, 1996b.

Smyth, S.B., et al., Factors influencing the upper free tropospheric distribution of reactive nitrogen over the South Atlantic during the TRACE-A experiment, *J. Geophys. Res., 101*, 24,165-24,186, 1996.

Thompson, A.M., The oxidizing capacity of the earth's atmosphere: Probable past and future changes, *Science, 256*, 1157-1165, 1992.

Thompson, A.M., K.E. Pickering, D.P. McNamara, M.R. Schoeberl, R.D. Hudson, J.H. Kim, E.V. Browell, V.W.J.H. Kirchhoff, and D. Nganga, Where did tropospheric ozone over southern Africa and the tropical Atlantic come from in October 1992? Insights from TOMS, GTE TRACE A, and SAFARI 1992, *J. Geophys. Res., 101/D19*, 24,251-24,278, 1996.

Turman, B.N., and B.C. Edgar, Global lightning distributions at dawn and dusk, *J. Geophys. Res., 87*, 1191-1206, 1982.

Vogt, R., P.J. Crutzen, and R. Sander, A mechanism for halogen release from sea-salt aerosol in the remote marine boundary layer, *Nature*, 383, 327-330, 1996.

Wang, Y., D.J. Jacob, and J.A. Logan, Global simulation of tropospheric O_3-NO_x-hydrocarbon chemistry: 1. Model formulation, *J. Geophys. Res., 103/D9*, 10,713-10,726 1998a.

Wang, Y., J.A. Logan, and D.J. Jacob, Global simulation of tropospheric O_3-NO_x-hydrocarbon chemistry: 2. Model evaluation and global ozone budget, *J. Geophys. Res., 103/D9*, 10,727-10,756, 1998b

Wang, Y., D.J. Jacob, and J.A. Logan, Global simulation of tropospheric O_3-NO_x-hydrocarbon chemistry: 3. Origin of tropospheric ozone and effects of non-methane hydrocarbons, *J. Geophys. Res., 103/D9*, 10,757-10,768, 1998c

Watson, C.E., J. Fishman and H.G. Reichle, The significance of biomass burning as a source of carbon monoxide and ozone in the southern hemisphere tropics: a satellite analysis, *J. Geophys. Res., 95*, 16,443-16,450, 1990.

Yienger, J.J., and H. Levy II, Empirical model of global soil-biogenic NO_x emissions, *J. Geophys. Res., 100*, 11,447-11,464, 1995.

Martin G. Schultz, Daniel J. Jacob, and Jennifer A. Logan, Department of Earth&Planetary Sciences, Harvard University, Cambridge MA 02138. (e-mail: mgs@io.harvard.edu; djj@io.harvard.edu; jal@harvard.edu)

Figure captions

Figure 1: Flight tracks of the DC-8 aircraft during PEM-Tropics A. Thin solid lines delineate the regions discussed in the text. Aircraft crossings of the intertropical convergence zone (ITCZ) and the South Pacific convergence zone (SPCZ) are indicated by tilde symbols.

Figure 2: Statistical distributions of ozone and CO mixing ratios at 4-8 km altitude in the 5 PEM-Tropics A regions defined in Figure 1. Horizontal lines are median values, boxes span the central 50% of the probability distribution, and the vertical lines cover the central 90%. The individual data are 1 minute averages

Figure 3: Median vertical profiles of mixing ratios for ozone, PAN, CO, and ethane observed over the equatorial and tropical South Pacific (0-30ºS, 170ºE-120ºW) during PEM-Tropics A, over the tropical northwestern Pacific (0-18ºN, 120ºE-170ºE) during PEM-West A, and over the tropical South Atlantic (0-25ºS, 30ºW-10ºE) during TRACE A. Also shown (dashed lines) are monthly mean September values from a global 3D model simulation [*Wang et al.,* 1998a] for the PEM-Tropics A region. Error bars for the PEM-Tropics A observations denote the central 50% range of the data, the grey shading represents the central 90% range of monthly mean 3D model concentrations for the ensemble of grid boxes over the equatorial and tropical South Pacific.

Figure 4: Modeled vs. observed NO_2/NO ratios in PEM-Tropics A (0-30ºS) as function of altitude. For explanation of the boxes and whiskers see caption of Figure 2. Only data with NO_2 photolysis frequencies greater than $7 \cdot 10^{-3}$ s^{-1} are displayed.

Figure 5: Ratio of 24-h average point model calculated chemical loss to chemical production rates for (a) H_2O_2 and (b) CH_3OOH in PEM-Tropics A (0-30ºS) as a function of altitude. See caption of Figure 2 for explanation of boxes and whiskers.

Figure 6: Mean chemical production and loss rates of NO_x calculated over the equatorial and tropical South Pacific during PEM-Tropics A (a: 0º-10ºS, b: 10ºS-30ºS). Values are 24-h averages. The model was constrained with concurrent observations of NO, HNO_3, and PAN. Rates of interconversion between NO_x and PAN are corrected for PAN-CH_3COO_2 cycling as described in the text.

Figure 7: Correlation between PAN and acetylene in the tropical south Pacific (10ºS-30ºS) during PEM-Tropics A at 4-8 km altitude.

Figure 8: Median profiles of (a) the chemical production rate, (b) the chemical loss rate, and (c) the net production rate (P-L) of ozone over the equatorial and tropical South Pacific during PEM-Tropics A. Values for the northwestern tropical North Pacific during PEM-West A [*Davis et al.,* 1996a], and the tropical South Atlantic during TRACE A [*Jacob et al.,* 1996] are shown for comparison. All values are 24-h averages. See caption in Figure 3 for region boundaries.

Figure 9: Mean ozone mixing ratios in ppbv over the tropical South Pacific for the month of September calculated by the Harvard/GISS global 3D model; (a) standard simulation, (b) simulation without biomass burning.

Plate 1: Geographical distribution of chemical production rates of ozone from the PEM-Tropics A data at 0-4.5 km and 4.5-12 km. Values are 24-h averages and are displayed on a $2^\circ \times 2.5^\circ$ grid.

Plate 2: Mean ozone production rates in September calculated by the Harvard/GISS global 3D model.

Table 1a: Median concentrations over the equatorial South Pacific (0-10ºS) in PEM-Tropics A.

	altitude band, km					
	0-2	2-4	4-6	6-8	8-10	10-12
observed quantities						
ozone, ppbv	12	23	38	32	37	31
NO_x, pptv	4	7	15	19	37	28
PAN, pptv	<1	2	19	23	32	19
HNO_3, pptv	23	59	74	52	59	27
H_2O_2, pptv	1410	1270	670	530	200	270
CH_3OOH, pptv	1170	840	360	250	80	110
CO, ppbv	55	53	53	57	61	57
ethane, pptv	245	265	290	280	300	290
propane, pptv	13	16	17	17	18	19
acetylene, pptv	16	18	25	28	31	34
point model results						
OH, 10^6 molec./cm^3	1.64	1.76	1.11	1.35	0.91	0.66
HO_2, 10^6 molec./cm^3	139	129	86	77	39	34
CH_3O_2, 10^6 molec./cm^3	234	166	69	37	13	11
HNO_4, pptv	< 0.1	0.1	1	5	19	16
CH_2O, pptv	340	220	130	100	50	40

Data collected in September-October 1996 over the equatorial regions shown in Figure 1. Model values are 24 h averages. This table contains 1430 values for species with 60s sampling time or less, 380 hydrocarbon samples, and 620 model runs.

Table 1b: Median concentrations over the tropical South Pacific (10ºS-30ºS) in PEM-Tropics A.

	altitude band, km					
	0-2	2-4	4-6	6-8	8-10	10-12
observed quantities						
ozone, ppbv	28	50	59	43	44	45
NO_x, pptv	3	22	26	18	58	98
PAN, pptv	1	19	89	43	48	42
HNO_3, pptv	18	145	155	60	65	47
H_2O_2, pptv	930	1040	620	560	240	130
CH_3OOH, pptv	880	480	250	310	90	< 35
CO, ppbv	58	68	70	59	63	58
ethane, pptv	310	380	400	340	350	360
propane, pptv	22	22	24	22	26	27
acetylene, pptv	52	67	68	51	52	53
point model results						
OH, 10^6 molec./cm^3	1.47	1.27	1.17	0.94	1.04	0.96
HO_2, 10^6 molec./cm^3	121	115	78	61	39	22
CH_3O_2, 10^6 molec./cm^3	217	90	49	33	13	5
HNO_4, pptv	< 0.1	0.7	3	5	28	29
CH_2O, pptv	280	200	125	80	65	50

Data collected in September-October 1996 over the tropical regions shown in Figure 1. Model values are 24 h averages. This table contains 3780 values for species with 60s sampling time or less, 1182 hydrocarbon samples, and 1387 model runs.

Table 2: Median 24-h average lifetimes for ozone and NO_x in PEM-Tropics A

	altitude band, km					
	0-2	2-4	4-6	6-8	8-10	10-12
ozone lifetime, days						
0º-10ºS	5	7	31	31	110	147
10ºS-30ºS	11	27	48	66	110	201
NO_x lifetime, days						
0º-10ºS	0.9	1.0	1.4	1.8	5.0	7.4
10ºS-30ºS	0.7	1.0	1.1	2.1	4.2	5.4

Table 3: Median 24-h average column budgets of O_x and CO in PEM-Tropics A

	P_{O3}	L_{O3}	$(P-L)_{O3}$	P_{CO}	L_{CO}	$(P-L)_{CO}$
0-12 km column						
0º-10ºS	1.36	3.20	-1.84	1.59	2.66	-1.07
10ºS-30ºS	1.82	3.05	-1.23	1.24	2.68	-1.44
0-16 km column						
0º-10ºS	1.72	3.24	-1.52	1.61	2.88	-1.27
10ºS-30ºS	2.18	3.09	-0.91	1.26	2.90	-1.64

Column rates of production (P) and loss (L) are in units of 10^{11} molec.cm^{-2}s^{-1}. At 12-16 km rates are computed by linearily extrapolating median concentration profiles above the 12 km ceiling of the aircraft. The extrapolated profiles for NO_x, ozone, and CO agree within 30% with observations from the STRAT (Stratospheric Tracers of Atmospheric Transport) campaign in August 1996 [*P. Wennberg*, personal communication, 1997].

Table 4: September mean ozone budget over the tropical South Pacific from the Harvard/ GISS global 3D model.

process	base simulation		no biomass burning	
	0-4.5 km	4.5-13 km	0-4.5 km	4.5-13 km
mean O_3 mixing ratio, ppbv	31	44	24	36
budget terms, 10^{11} molec.cm^{-2}s^{-1}				
advection from west	-0.33	+3.84	-0.26	+2.70
from east	+1.81	-2.51	+1.03	-1.85
from south	-0.14	-0.92	-0.07	-0.65
from north	-0.19	+0.04	-0.08	+0.04
total (flux divergence)	+1.14	+0.46	+0.62	+0.24
vertical transport	+0.53	-0.49[a]	+0.50	-0.46[a]
chemical production	+0.98	+0.92	+0.52	+0.74
chemical loss	-2.61	-0.71	-1.63	-0.48
dry deposition	-0.27	0	-0.20	0
residual[b]	-0.23	+0.18	-0.19	+0.04

The budget was computed for the region 0-28ºS, 165ºE-100ºW. Fluxes are normalized to horizontal surface area. Positive transport terms indicate net inflow.

[a] includes direct input from the stratosphere

[b] diffusive transport and tendency term

Figure 1

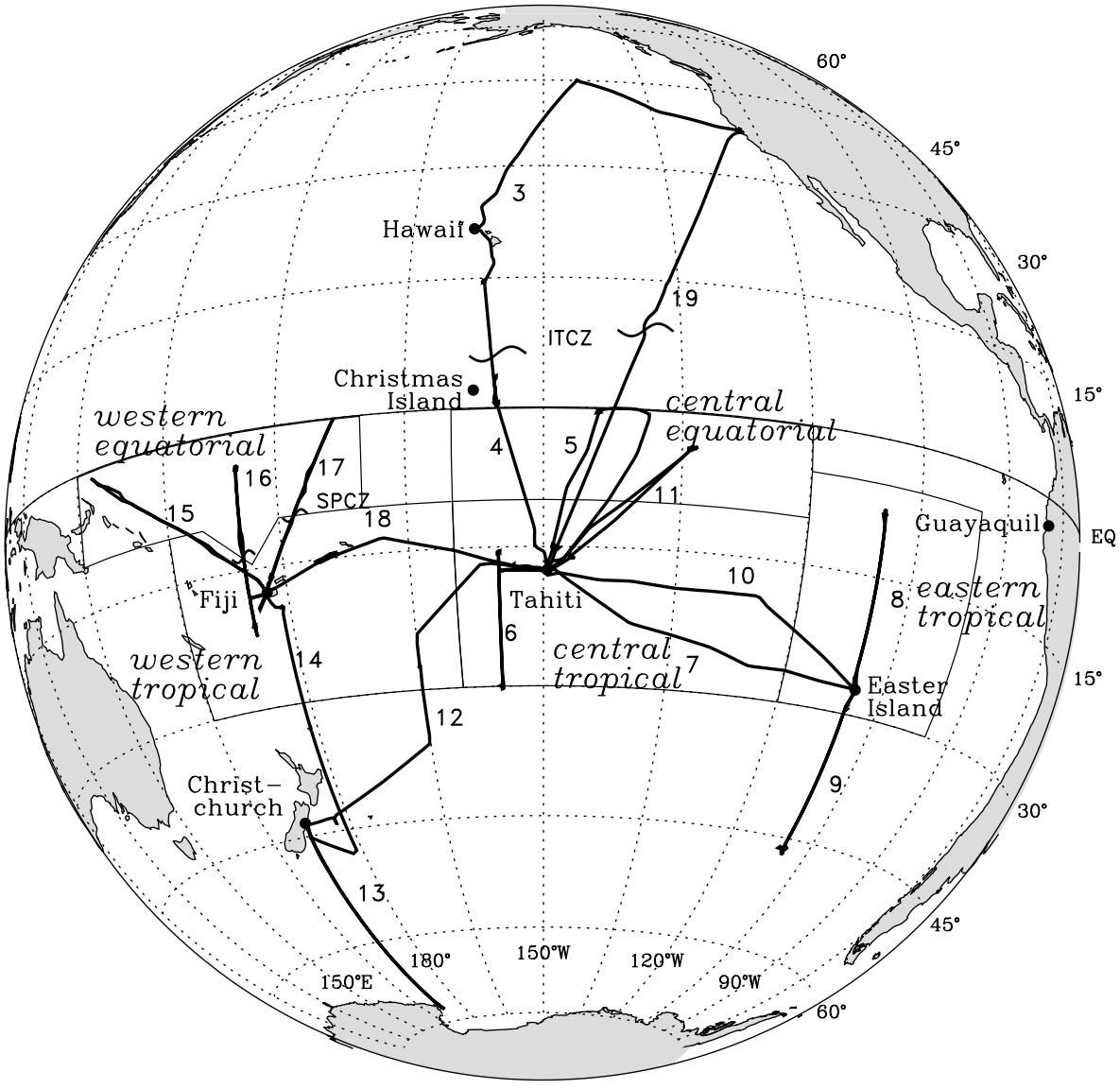
60°
45°
30°
15°
EQ
15°
30°
45°
60°
Hawaii
Christmas Island
ITCZ
SPCZ
Fiji
Tahiti
Guayaquil
Easter Island
Christ-church
western equatorial
central equatorial
eastern tropical
western tropical
central tropical
3
19
4
5
16
17
15
18
11
10
8
6
7
14
12
9
13
180°
150°W
120°W
90°W
150°E

Figure 2

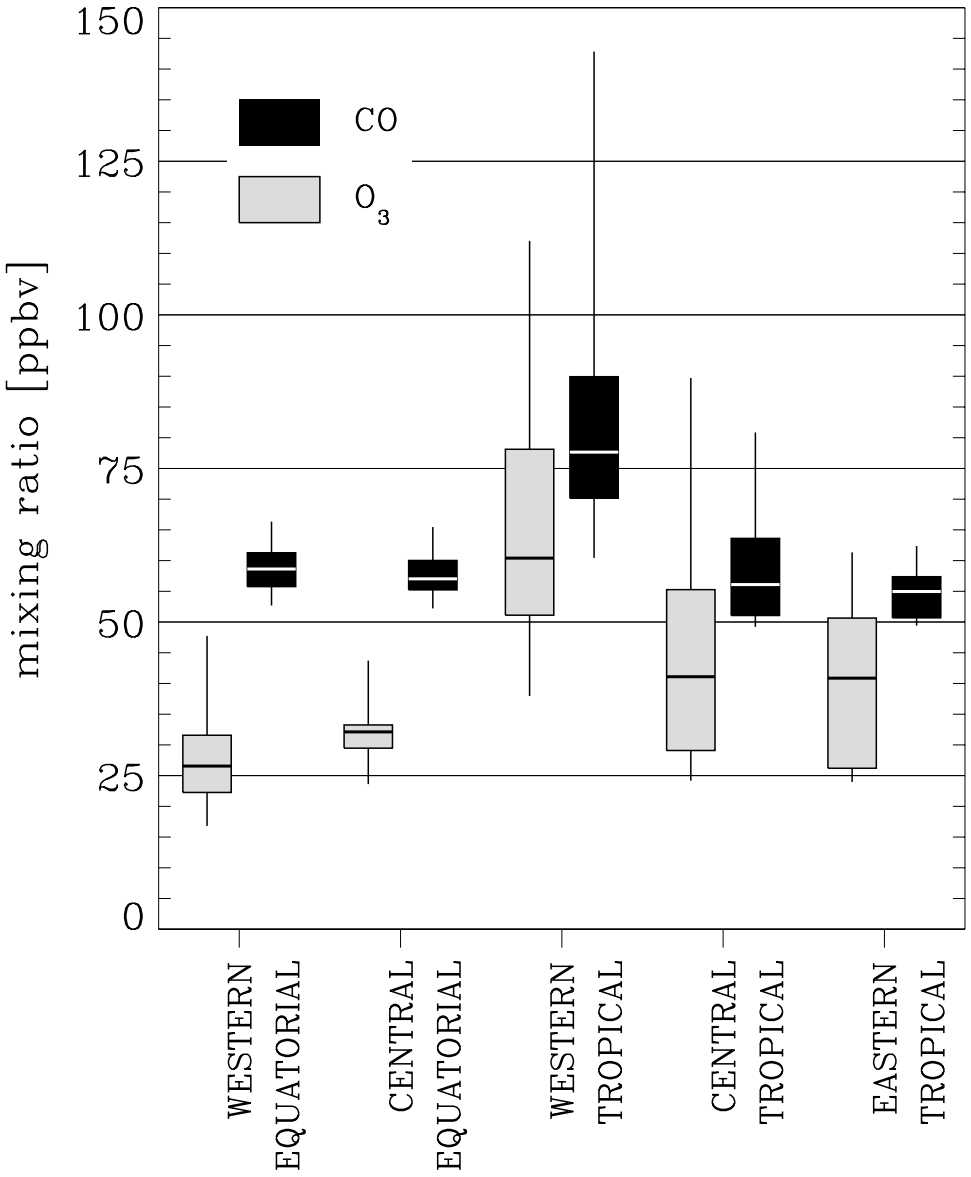
150
125
100
75
50
25
0
mixing ratio [ppbv]
CO
O3
WESTERN EQUATORIAL
CENTRAL EQUATORIAL
WESTERN TROPICAL
CENTRAL TROPICAL
EASTERN TROPICAL

Figure 3

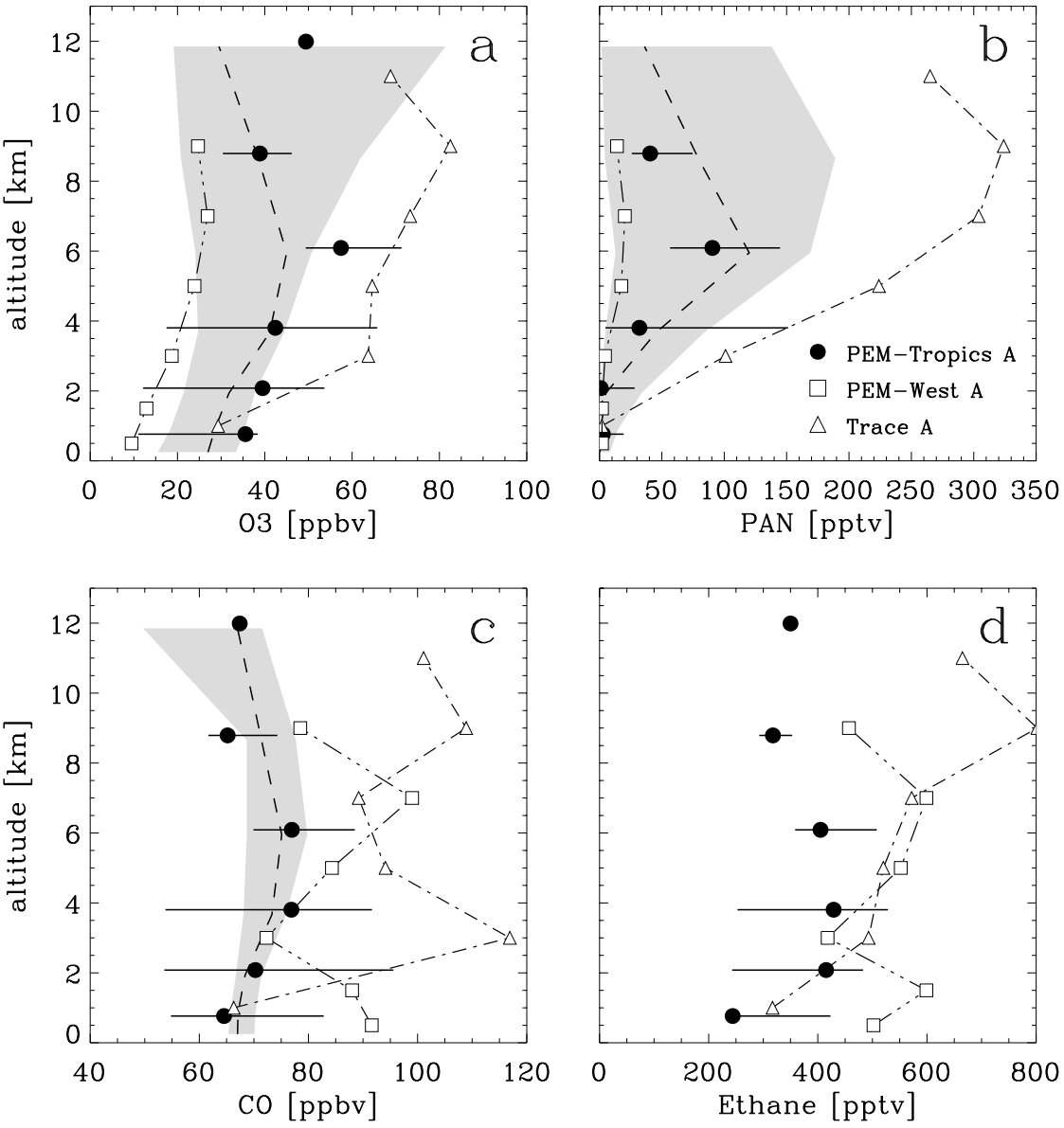
a
b
c
d
altitude [km]
O3 [ppbv]
PAN [pptv]
CO [ppbv]
Ethane [pptv]
PEM−Tropics A
PEM−West A
Trace A

Figure 4

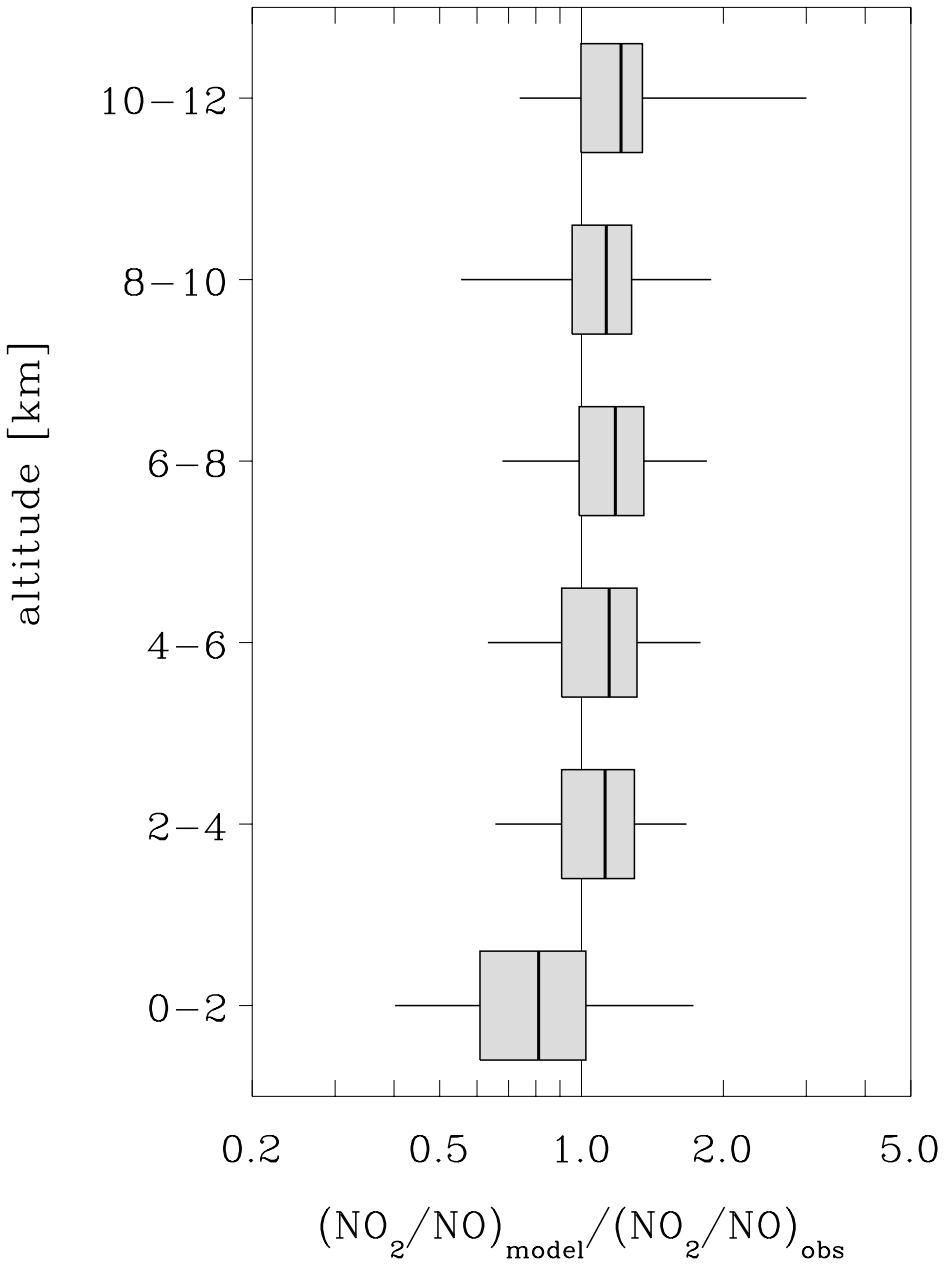
10−12
8−10
6−8
4−6
2−4
0−2
altitude [km]
0.2
0.5
1.0
2.0
5.0
(NO2/NO)model/(NO2/NO)obs

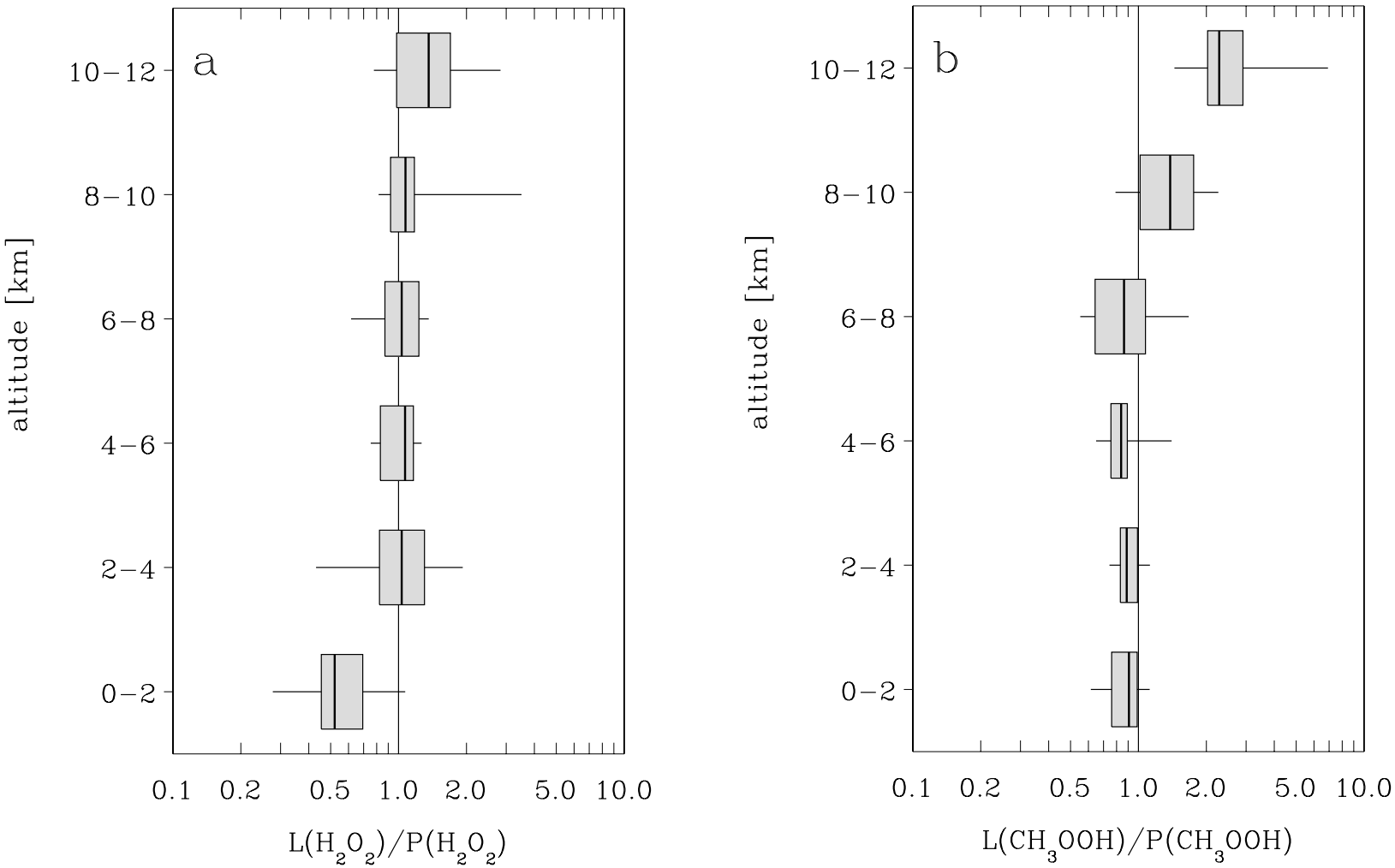
a
b
altitude [km]
10–12
8–10
6–8
4–6
2–4
0–2
0.1
0.2
0.5
1.0
2.0
5.0
10.0
L(H2O2)/P(H2O2)
L(CH3OOH)/P(CH3OOH)

Figure 5

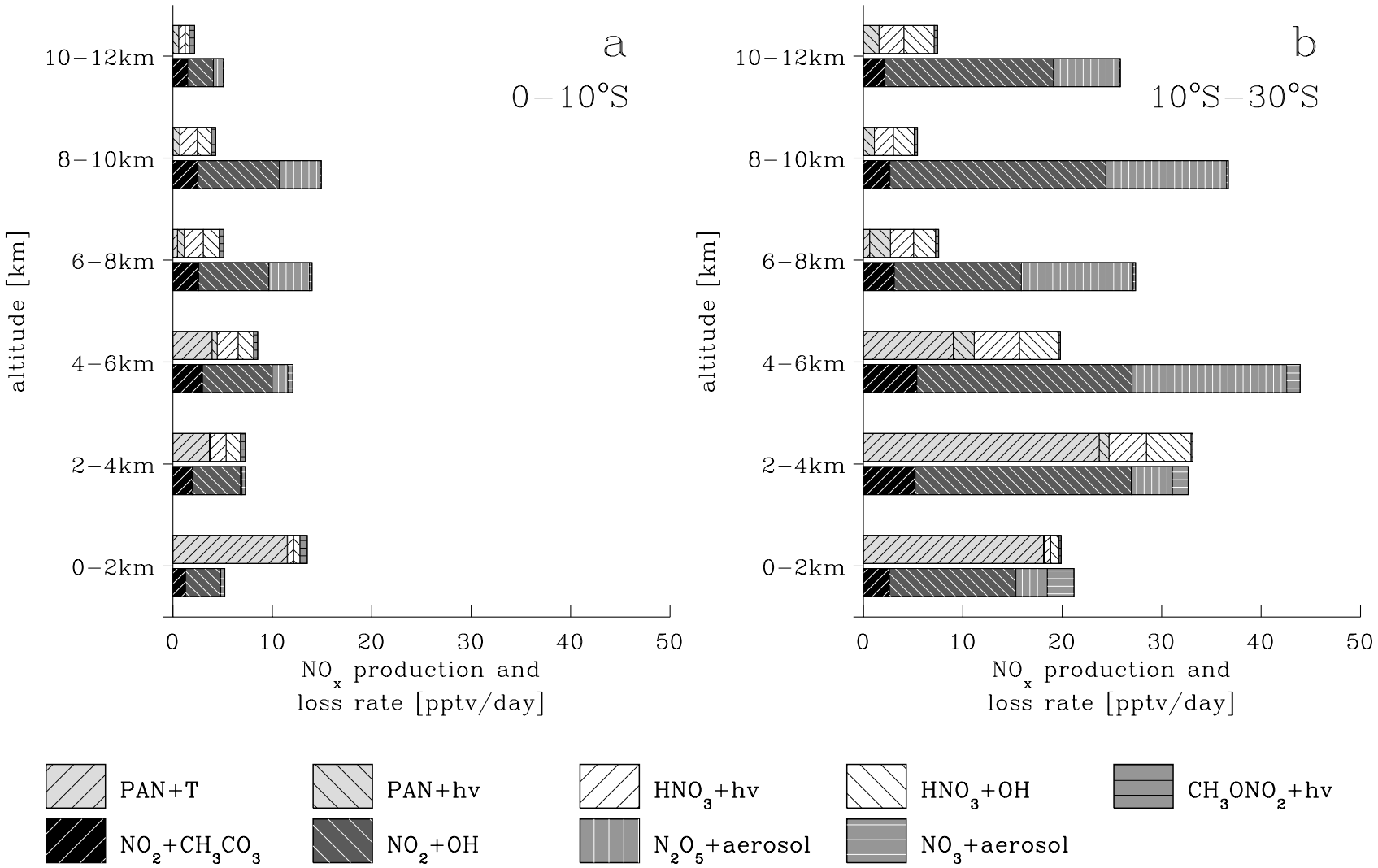
a
0−10°S
b
10°S−30°S
10−12km
8−10km
6−8km
4−6km
2−4km
0−2km
altitude [km]
0
10
20
30
40
50
NOx production and
loss rate [pptv/day]
PAN+T
PAN+hv
HNO3+hv
HNO3+OH
CH3ONO2+hv
NO2+CH3CO3
NO2+OH
N2O5+aerosol
NO3+aerosol

Figure 6

Figure 7

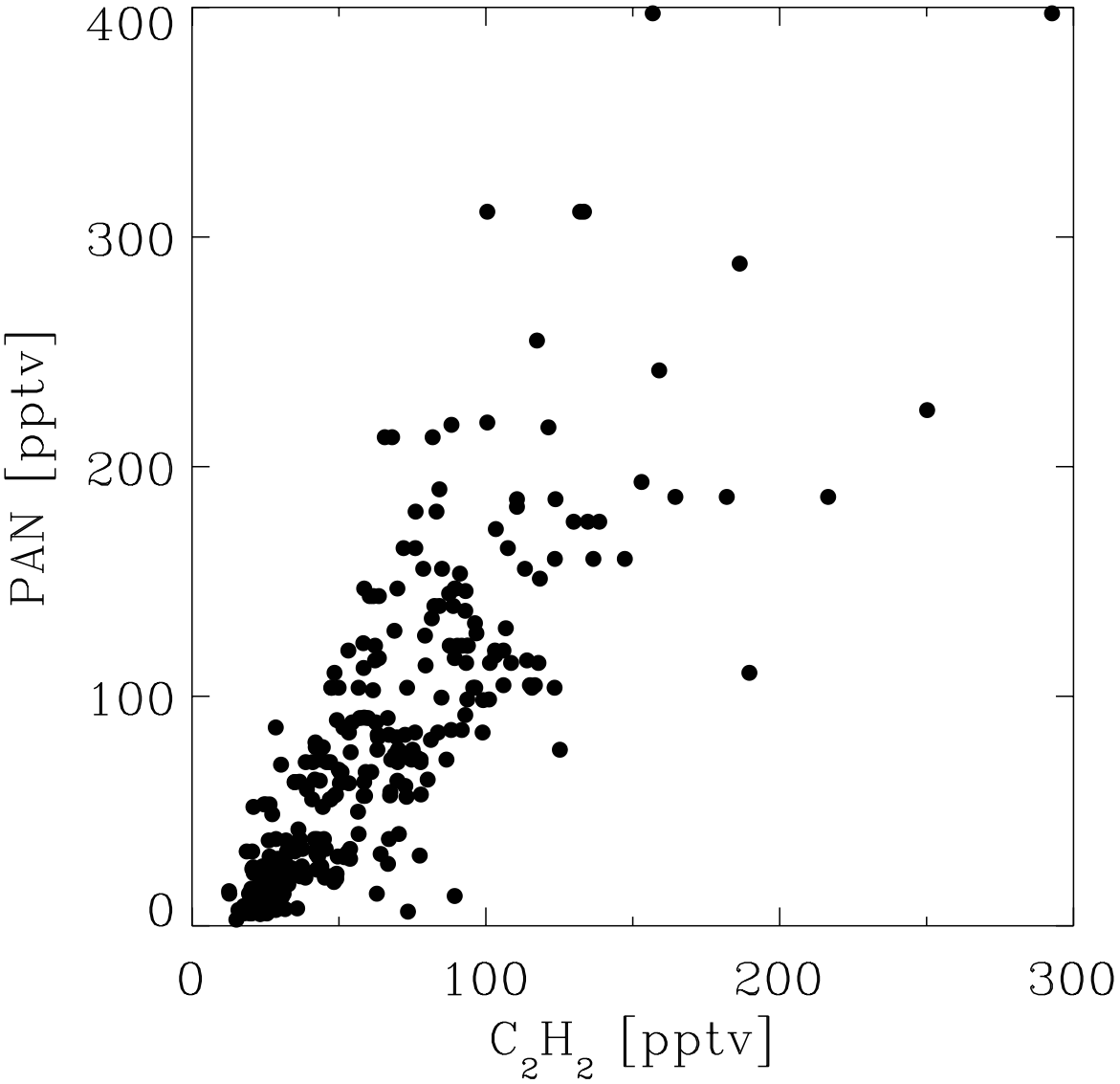

Figure 8

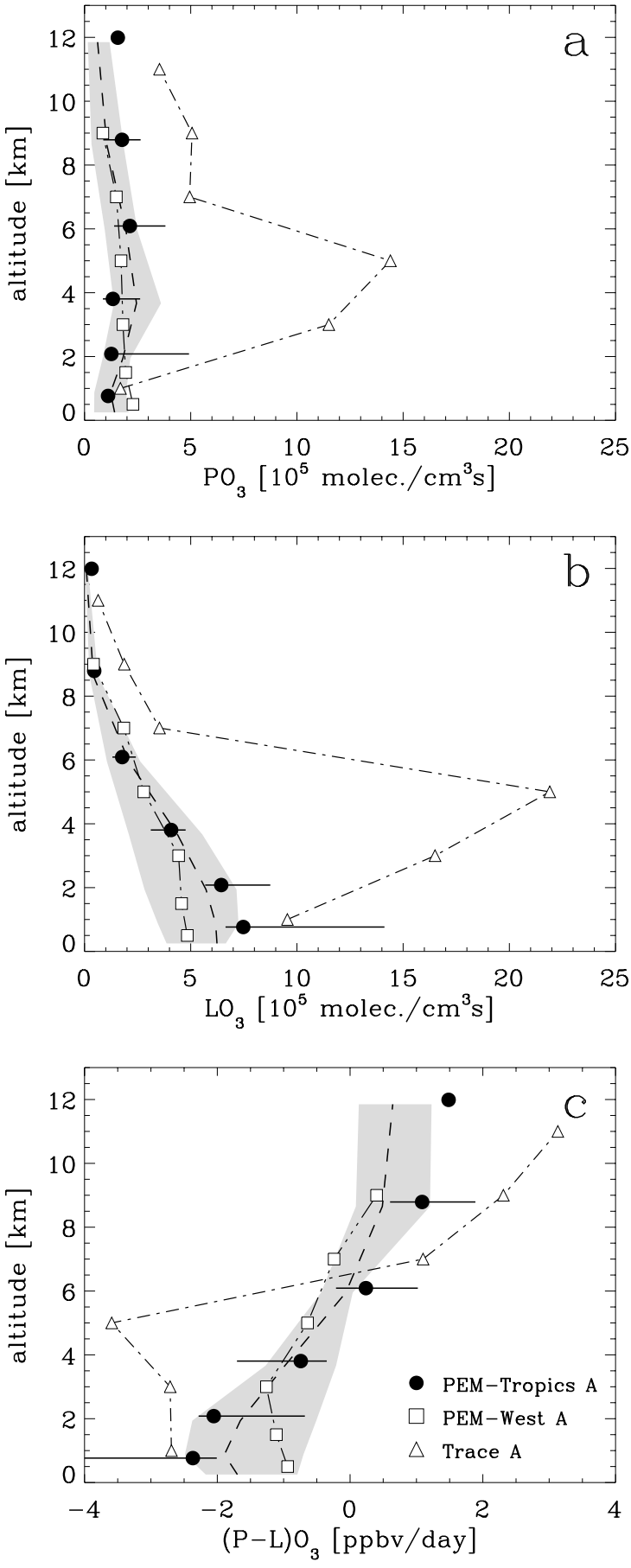
a
altitude [km]
PO3 [10^5 molec./cm^3s]
b
altitude [km]
LO3 [10^5 molec./cm^3s]
c
altitude [km]
(P−L)O3 [ppbv/day]
PEM−Tropics A
PEM−West A
Trace A

Figure 9

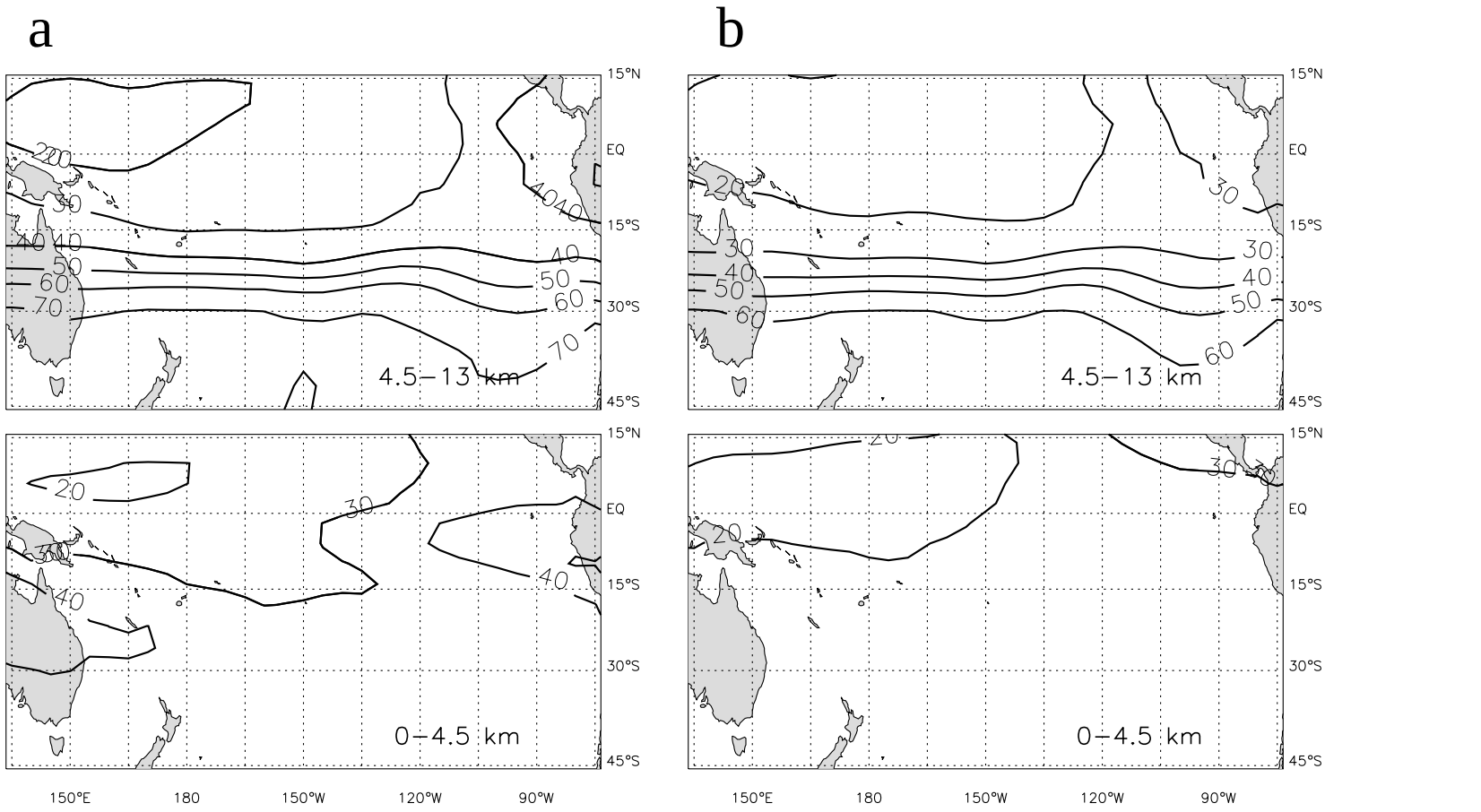

03

Plate 1

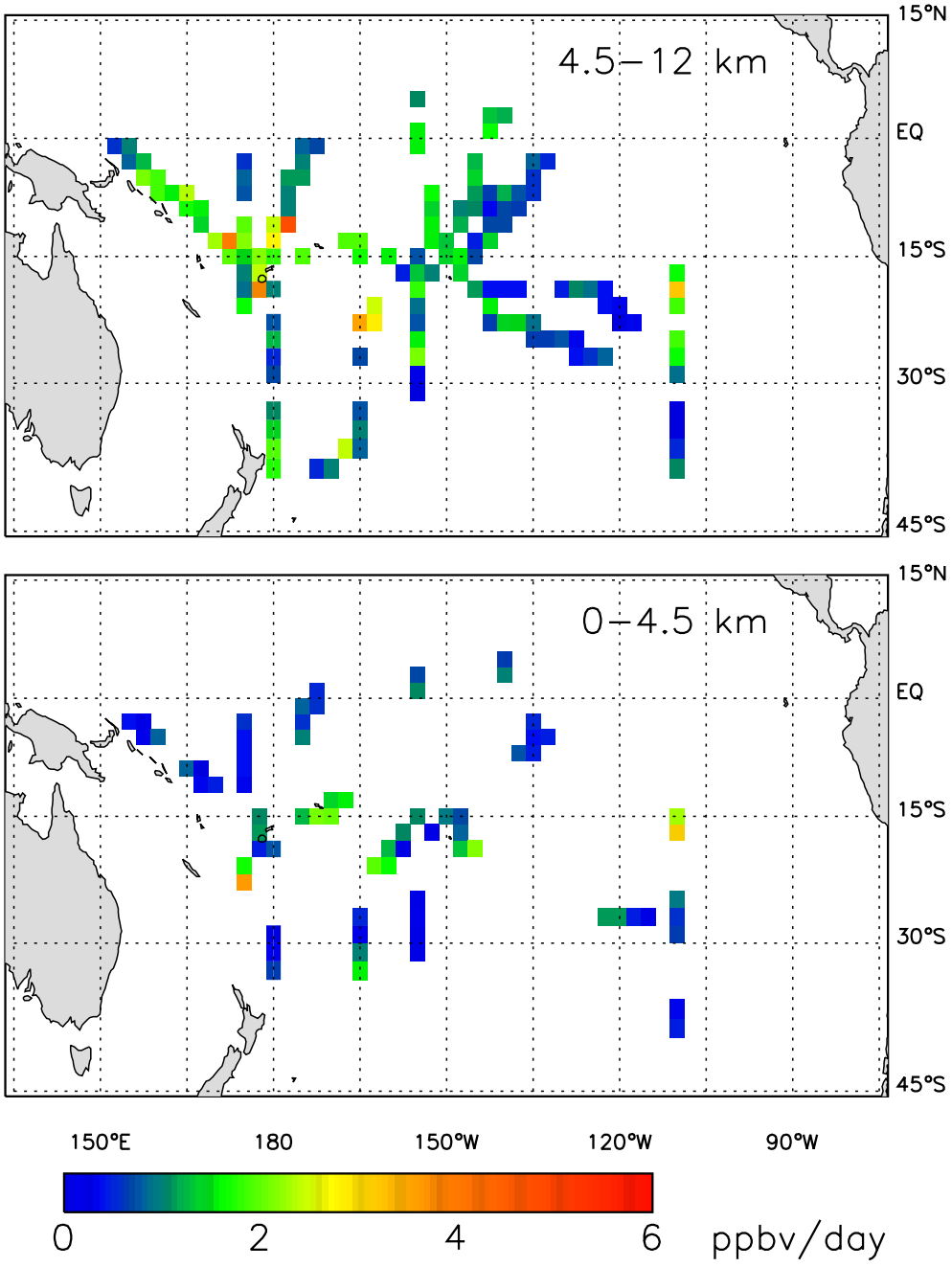
4.5–12 km
0–4.5 km
15°N
EQ
15°S
30°S
45°S
150°E
180
150°W
120°W
90°W
0
2
4
6
ppbv/day

Plate 2

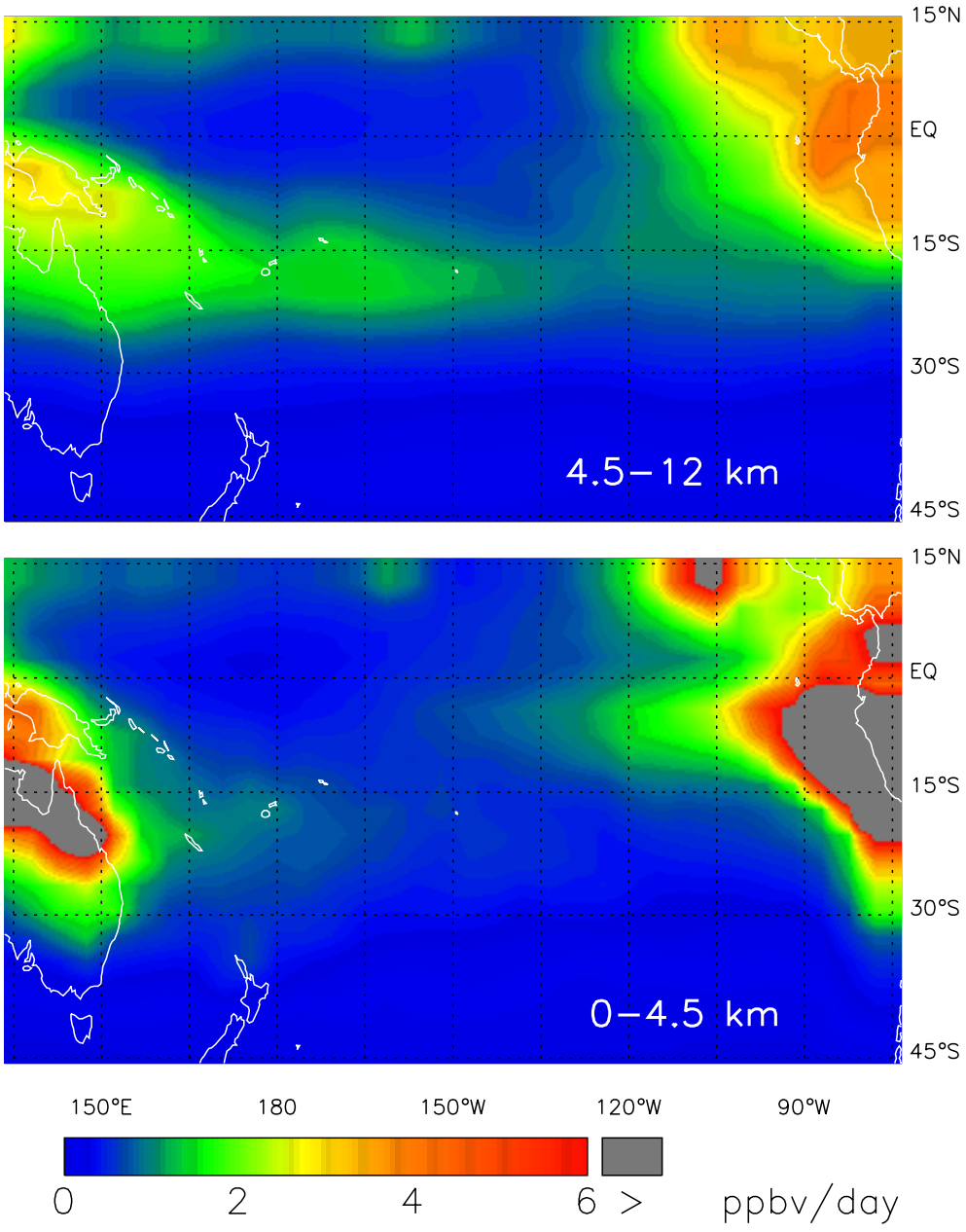
15°N
EQ
15°S
30°S
45°S
4.5–12 km
15°N
EQ
15°S
30°S
45°S
0–4.5 km
150°E
180
150°W
120°W
90°W
0
2
4
6 >
ppbv/day